Original scientific paper

MICROSTRUCTURE INFLUENCE ON FRICTION BEHAVIOR OF THE TI6AL4V BIOMEDICAL ALLOY AT LOW LOADS

Fatima Zivic[1], Slobodan Mitrovic[1], Petar Todorovic[1], Dragan Adamovic[1], Nenad Grujovic[1], Marko Spasic[2], Ivan Stojadinovic[3]

[1]University of Kragujevac, Faculty of Engineering, Kragujevac, Serbia
[2]University of Kragujevac, Faculty of Medical Sciences, Department of Surgery, Kragujevac, Serbia
[3]Clinic for Orthopedics and Traumatology, University Clinical Center, Kragujevac, Serbia

Abstract. *Dynamic friction coefficient (COF) between Ti6Al4V and Al_2O_3 was analyzed under low loads (100 mN, 250 mN, 500 mN, 750 mN, 1000 mN), sliding speed (4 mm/s, 8 mm/s, 12 mm/s) at dry contact and in the Ringer's solution. Different Ti6Al4V microstructures were studied: Sample 1 - fully lamellar; Sample 2 - martensitic; sample 3 - equiaxed; and sample 4 - globular microstructure. The maximum COF values varied as: 0.4 - 1.23 (Sample 1), 0.5 – 2.8 (Sample 2), 0.4 – 1.1 (Sample 3), and 0.4 – 2.3 (Sample 4). Lamellar and martensitic microstructures were not beneficial for the tribological response since they exhibited severe wear and very high COF values. The globular Ti alloy microstructure showed extremely high COF and wear under dry conditions. In general, water quenching was not a favorable treatment for tribological behavior. The lowest COF values and wear volumes were exhibited in the case of equiaxed microstructure.*

Key Words: *Ti6Al4V, Friction Coefficient, Tribochemical Wear, Reciprocating Sliding*

1. INTRODUCTION

Biomedical applications of Ti alloys are broad and extensive due to their high strength, low density, high corrosion resistance, excellent biocompatibility and elastic modulus that can be tailored close to the one of the bone [1, 2]. However, even with extensive research on processing parameters during production and different thermo-mechanical processing [3, 4, 5, 6], Ti alloys still exhibit certain drawbacks that prevent their wider application as implant materials. The major problem with these alloys is a low wear resistance [7],

especially under variable contact conditions including elevated temperatures. High temperatures significantly change the mechanical properties of Ti alloys [8]. Thermal softening, during the contact, depending on the load and velocity, is proven for Ti alloys [9], thus greatly influencing friction and wear response of the material. Mechanical properties of Ti alloys (tensile behavior and especially the yield strength) are closely related to their microstructure, including multi-scale microstructural properties (like precipitates, regions of different microtextures and their distribution along with dynamic complex changes under external stresses) [10, 11, 12, 13]. Changes in the microstructure due to the heat treatments, or some other dynamic process, can result in rather different mechanical behavior even in the case of similar initial microstructures [10, 14, 8, 15]. Variation of heat treatment parameters can enable tailoring of different microstructures [5, 4, 16]. Dynamic processes at α/β interfaces under deformation have significant influence on the resulting mechanical behavior of Ti alloys [17]. Tribological contact also provokes different microstructural changes within the surface layers [18, 19, 20, 21]. Different contact environments introduce additional influential factors from chemical and tribochemical processes that develop during the tribological contact [22]. Ti alloys are highly reactive and prone to different chemical reactions, especially in corrosive and aggressive environments [14, 23]. For example, presence of hydrogen can cause severe embrittlement under deformation [24].

Altogether, this makes a very complex and difficult task to predict and design good mechanical response of the Ti alloys for all load bearing applications where the tribological contact is present, thus limiting the use of this otherwise excellent biomaterial. Standard Ti6Al4V alloy is widely used in total hip arthroplasty [25, 26], but challenges related to the stress distribution (stress shielding) and poor contact wear resistance, largely focus its application to the stationary femoral stem and acetabular components [27, 28, 29].

During the last decades several ASTM standards were adopted, pertaining to Ti6Al4V alloy for medical applications: ASTM F1472 – 14, ASTM F1108 – 14, ASTM F136 – 13, ASTM F2885-17, ASTM F2146-13, ASTM F620-11(2015), ASTM F3001-14, ASTM F2193-20. They provide guidelines and recommendations on the optimal processing routes and parameters to obtain the best microstructure, from aspects of its applications. However, friction and wear mechanisms are still under investigations, focusing on the possibilities to surpass the previously listed shortcomings related to the wear resistance. Comprehensive review of Ti alloy properties is given in [1, 2]. Review of different Ti6Al4V microstructures depending on the processing parameters is presented in [30], along with mechanisms that govern tribological behavior under various dry conditions. They analyzed tribo-oxidation layers and wear mechanisms associated with it. They also reviewed research related to strain rate response, also in conditions of elevated temperature and frictional heating, which leads to significant changes of Ti6Al4V microstructure in surface layers and further contribute to changes of wear mechanisms. Extensive research has been done related to production routes and processing of Ti alloys, in order to obtain the most favorable microstructures from aspect of wear resistance [2, 3], and new additive manufacturing technologies have emerged to enable better tailoring of properties [31, 32, 33, 27, 29].

Friction causes high flash temperatures in the contact zone [34, 35], especially for the dry sliding, thus decreasing the resistance to plastic shearing in Ti alloys; different models have been investigated [36, 37, 38]. Surface oxides created during the contact, due to reactions with counterbody material and environment, greatly influences wear and friction

behavior. In some cases TiO_2 passive film can be formed on Ti6Al4V that protects the surface from wear [39]. Other Ti oxides can be found (Ti_2O_3, TiO_2) and depending on the counterbody material, very hard and sharp TiAl intermetallics have also been proven (Ti_3Al, TiAl, and $TiAl_3$) that increase wear rate [40, 41]. Distribution and size of α and β phases govern the damage mechanisms during the loading while the changes in the microstructure result in different material responses [42, 23]. High flash temperatures that appear within the limited contact zones, due to friction, rapidly decrease Ti6Al4V yield strength and result in localized material softening [43, 41]. It is further favorable for mechanical alloying of the materials in contact. Altogether, it results in complex dynamic changes of Ti6Al4V microstructures in surface layers during the tribocontacts. Both wear and friction can exhibit transition feature during certain contact conditions [39, 40]. Research on underlying mechanisms to these complex dynamic processes is still ongoing.

This paper presents experimental data and analysis pertaining to the friction and wear mechanisms during reciprocating sliding of Ti6Al4V with four different microstructures against Al_2O_3, under low loads and different sliding speeds. We varied five values of load, three values of sliding speed and two different contact environments (dry contact and contact in the Ringer's solution), and analyzed friction and wear mechanisms. The efficient friction coefficient (COF_{eff}) that numerically represents the whole COF curve was introduced in the evaluation of friction results.

2. MATERIALS AND EXPERIMENTAL METHODS

2.1 Materials

Ti6Al4V alloy flat samples were cut from commercial Ti6Al4V alloy bars and subjected to four types of heat treatments, as described in [42, 23]. Ti6Al4V ELI (Extra Low Interstitials) (Grade 23) was used as one of the main materials for orthopedic implants, with good fracture toughness due to the lowered oxygen content in comparison to the commercial Ti6Al4V alloy (Grade 5). Four types of samples were produced, by annealing them in Ar for 1h, at two different temperatures, followed by two different cooling methods and rates (slow cooling in furnace and rapid cooling by water quenching), as follows:
- − Sample 1 - annealed at 1000°C; furnace cooled, with fully lamellar microstructure,
- − Sample 2 - annealed at 1000°C; water quenched, with martensitic microstructure,
- − Sample 3 - annealed at 750°C; furnace cooled, with equiaxed microstructure,
- − Sample 4 - annealed at 750°C; water quenched, with globular microstructure.

Final polishing and cleaning were done in accordance with ASTM F86, as described in [7]. The final roughness was Ra=0.07μm. The material in contact with all Ti samples was alumina ball (Al_2O_3), commercially supplied by Anton Paar Company. Aluminum oxide is a chemically inert material, with excellent abrasion resistance and significantly harder than Ti alloys, which should provide that the material changes during tribocontacts are to be attributed only to the Ti alloy.

2.2 Tribological Tests

Comprehensive tribological tests were realized, by using linear reciprocating sliding module (tribometer from Anton Paar, model CSM nanotribometer), with details of the

device setup and parameters given in [7]. All Ti alloys were subjected to 30000 cycles (0.5mm stroke), in contact with alumina ball (1.5 mm diameter) and with variation of the following test parameters: five different loads (100mN, 250mN, 500mN, 750mN, 1000mN), three different maximum sliding speeds (4mm/s; 8mm/s; 12mm/s) and two different contact environments (dry contact and contact in The Ringer's solution), at the room temperature. Composition of the Ringer solution used is as follows (g per 1 liter of water): NaCl - 8.6; KCl - 0.30; $CaCl_2$ - 0.33; Na+ 147.00 mmol; K+ 4.00 mmol; Ca+ 2.25 mmol; Cl+ 155.60 mmol. In the case of the wet contact, the whole contact zone was fully immersed in fresh Ringer's solution, for each of the tests. 30000 cycles accounted for approximately up to 3.6h depending on the nature of the friction coefficient of the investigated sample.

During each test, a nanotribometer-recorded dynamic friction coefficient values in real time, with 100Hz sampling frequency. The device also recorded values of the penetration depth of alumina ball into flat Ti samples, during the contact, with the same sampling frequency. Details of the penetration depth parameter changes and wear are given in [7, 42]. Images of the worn tracks on Ti samples were taken by optical and SEM microscopy (MEIJI MT8530, MEIJI MC 50T microscopes and JEOL JSM-6610LV SEM microscope).

The dynamic friction coefficient is represented by the continuous curve showing values of friction coefficient at discrete points of time during the test, depending on the adopted sampling frequency. For 100Hz sampling frequency, there are numerous recorded values of the discrete friction coefficients for one test (100 values each second during the test), as output results from the nanotribometer. The sine wave shape of the *COF* curve (Fig. 1) enables processing of the raw data signal in several ways aiming to filter the signal for easier interpretations. It is possible to calculate one numerical value, the efficient friction coefficient (COF_{eff}) that will numerically represent the whole *COF* curve, by applying averaging and root mean square of the *COF* function. In such way, the complex *COF* curve is reduced to one number, COF_{eff} that corresponds well with frictional behavior of the contact pair and can rapidly show specific trends with changes of the contact load and speed. Detailed discussion of COF_{eff} is given in [44] and it is calculated according to the following equation:

$$COF_{eff} = \sqrt{\frac{COF_1^2 + COF_2^2 + COF_3^2 + ... + COF_n^2}{n}} \qquad (1)$$

where, COF_{eff} is the numerical value (root mean square of the *COF* function for one test), COF_i is the numerical *COF* value recorded by the device at i-point of time and *n* is the total number of points at which *COF* was recorded during one test.

3. RESULTS AND DISCUSSION

The dynamic friction coefficient (*COF*) for 10 cycles (laps), as extracted from one test (Sample 1, dry contact, v=4 mm/s; FN=100mN) is shown in Fig. 1. It can be seen that, in general, the dynamic friction coefficient curve is of sinusoidal shape. The peak values show a strongly oscillating behavior. All the friction curves at all the tests have similar dynamic nature, with a few peaks at the maximum *COF* values over time, as shown in Fig. 1.

Fig. 1 Dynamic friction coefficient for 10 cycles (test duration of 3.93s) (Sample 1, dry contact, 4 mm/s, 100mN)

The peak values of the friction curve represent the maximum values of the friction coefficient, at the moment when the friction force is of the maximum value. It corresponds closely to the change of sliding direction, considering that this is a linear reciprocating motion of the ball over the flat Ti alloy surface (simulation of the point contact, or Hertzian contact). The shape of the friction coefficient curve and its peaks reflect the stopping and moving of the ball in opposite direction. Accordingly, it exhibits stick-slip effects of the local running-in for a very short period, when the ball changes its direction of sliding. This is a very short time when the system transits from static state to kinetic state. When the ball is stopped for a very short period of time, microscopic junctions that are continuously formed and broken during the dynamic contact between the surface asperities of the contact pair, become stronger and stick-slip occurs, as clearly shown by the peaks in Fig. 1. These brief local running-in periods continuously occurred during the steady-state of the dynamic friction coefficient, for all test conditions. General sine wave shape of the dynamic friction coefficient allows different methods of processing of such signal [44]. Calculations of average and maximum values, along with some degree of filtering, are common practice with sine waves. On the other hand, dynamic coefficient curves of the whole test can be analyzed from different aspects, such as initial running-in period, steady state, occurrence of abrupt variation of values in steady state, or different periods within steady state (mean and maximum *COF* values within these periods or increasing/decreasing trends of maximum *COF* values). Each of these indicates some phenomena during the sliding contact, thus altogether resulting in complex interpretation of the whole dynamic friction coefficient behavior, especially at micro and nano scale.

Selected real time diagrams of the dynamic friction coefficient, with related wear tracks, for each of the four samples, are shown in Figs. 2-5. Regimes of low load and low sliding speed, in comparison with the high load and high speed, are shown and compared in these images, as representatives of the two opposite contact conditions. Also, the comparison of dry contact to the contact in the Ringer's solution, for the same speed and load, is shown in each of the Figs. 2-5. The relevant wear mechanisms of these samples

and contact conditions are discussed in our previous papers [7, 42]. Wear mechanisms and corrosion induced damage behavior during the contact between the same materials as in our study, under higher loads and different contact geometry, were analyzed in these articles [45, 46]. Comprehensive review of wear mechanisms related to Ti6Al4V alloy, under different contact conditions, is given in [30]. Frictional behavior is closely related to the wear and damage mechanisms that govern the contact.

The *COF* curves in Figs. 2-5 appear as a surface due to a long test period (30000 cycles), but when zoomed to a short time period, the shape of each curve is similar to the one shown in Fig. 1. Nanotribometer simultaneously provides total time [s], total distance [mm] and number of cycles [lap], as shown in Fig.1. Especially the total time is a useful parameter because it indicates the friction force level, in general. Namely, for 30000 cycles, each test condition had different total times, strongly depending on both the sliding speed and normal load that were applied in the test. In Figs. 2-5, horizontal axes show the total time needed to complete the 30000 cycles of the reciprocating linear sliding tests. Each *COF* curve is shown next to the related wear track after the test is finished. Each of the figures shows dry contact (Figs. 2-5a, b) and contact in the Ringer's solution (Figs. 2-5c, d), for one sample. This was a comprehensive experimental study that was realized during one year to complete all tests and these results are representative of the observed trends for the sliding contact between Ti6Al4V and alumina, under micro-scale loads.

The maximum *COF* values for all samples were significantly larger under low loads and low speeds, then under high loads and high speeds. The *COF* values significantly decreased for the highest load and speed (1000 mN, 12 mm/s). For all the samples, except in the case of Sample 2, wear tracks were significantly larger under low load/speed than under high load and speed. However, regarding wear, uniform trend for all loads cannot be defined, as discussed in [7, 42]. Contact conditions with the lowest load (100 mN) and the highest load (1000 mN) exhibited significantly different values for both the friction coefficient and wear volumes, as shown in Figs. 2-5. The smallest wear track together with the lowest wear volumes were exhibited for the highest load (1000 mN) and sliding speed (12 mm/s), for all samples. For the sliding in the Ringer's solution, all the *COF* curves were fully uniform without variation of maximum values, from the start until the end of test, almost without the running-in period, except for a very short initial period (order of a few seconds). Maximum *COF* values (for both dry and wet contacts) varied within the ranges: 0.4 - 1.23 (for Sample 1), 0.5 – 2.8 (for Sample 2), 0.4 – 1.1 (for Sample 3), and 0.4 – 2.3 (for Sample 4). In the case of the Sample 1, under the lowest load and speed (100 mN, 4 mm/s), the maximum *COF* values exhibited a slight increase over time, with periodic small variations within very short periods. Wear tracks were of similar sizes, except in the case of dry sliding under 100 mN load and 4 mm/s speed, which is significantly larger (Fig 2a), indicating severe abrasive wear, with coarse wear debris particles surrounding the wear track.
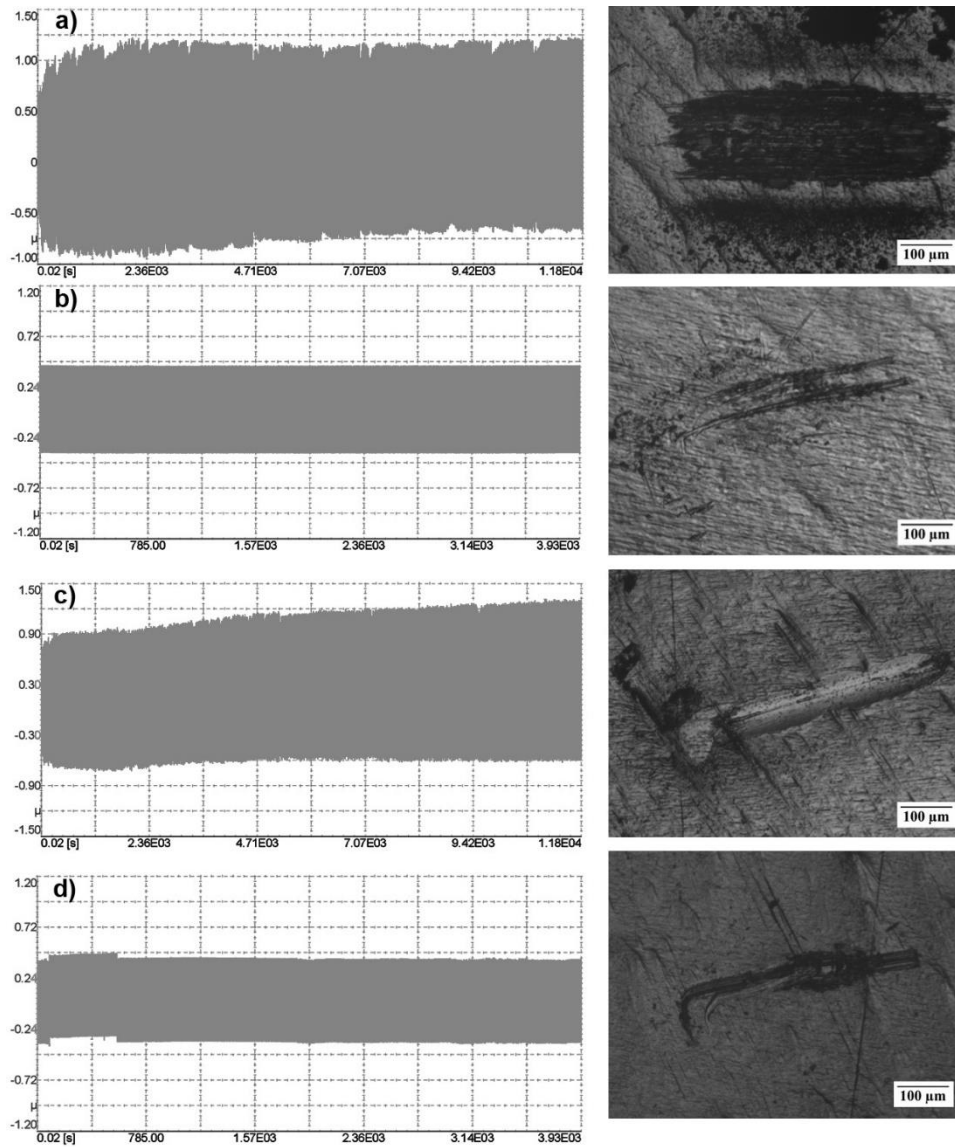
Fig. 2 Sample 1: Dynamic friction coefficient (left) and related wear tracks (right): a) Dry, v=4 mm/s; FN=100mN, b) Dry, v=12 mm/s; b FN=1000mN, c) Ringer, v=4 mm/s; FN=100mN, d) Ringer, v=12 mm/s; FN=1000mN

For Sample 2, low load and speed (100 mN, 4 mm/s) resulted in an extremely high increase of the *COF* values over longer time, especially in dry conditions (Fig. 3a, c).
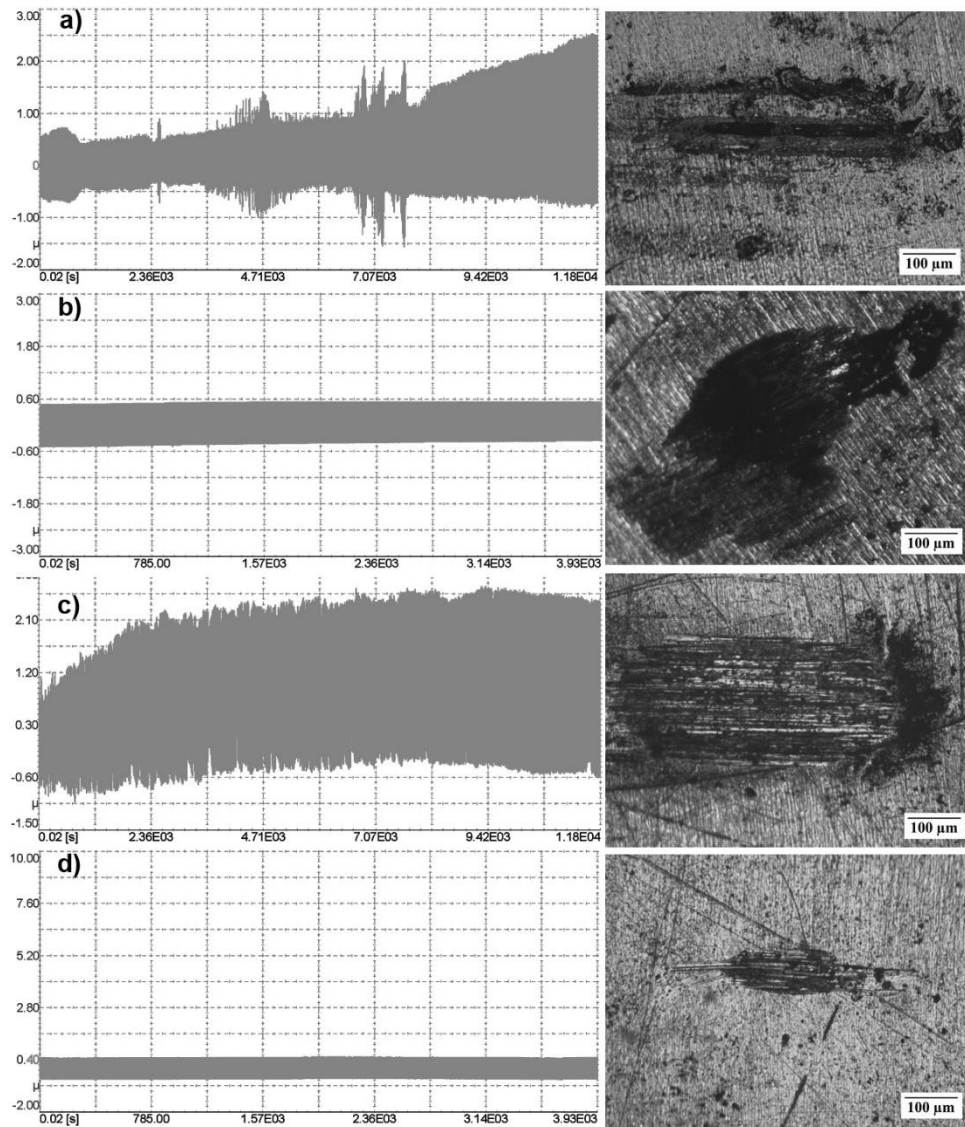
Fig. 3 Sample 2: Dynamic friction coefficient (left) and related wear tracks (right): a) Dry, v=4 mm/s; FN=100mN, b) Dry, v=12 mm/s; b FN=1000mN, c) Ringer, v=4 mm/s; FN=100mN, d) Ringer, v=12 mm/s; FN=1000mN

Increase of load decreased the *COF* values. Same conditions in the case of Sample 2 resulted in lower wear rate for wet contacts, especially under higher loads (wear rates were discussed in [7, 42]). This is in accordance with experimental tests in [45] where Sample 2 subjected to block-on-disk contact configuration in the Ringer's solution, at high loads and

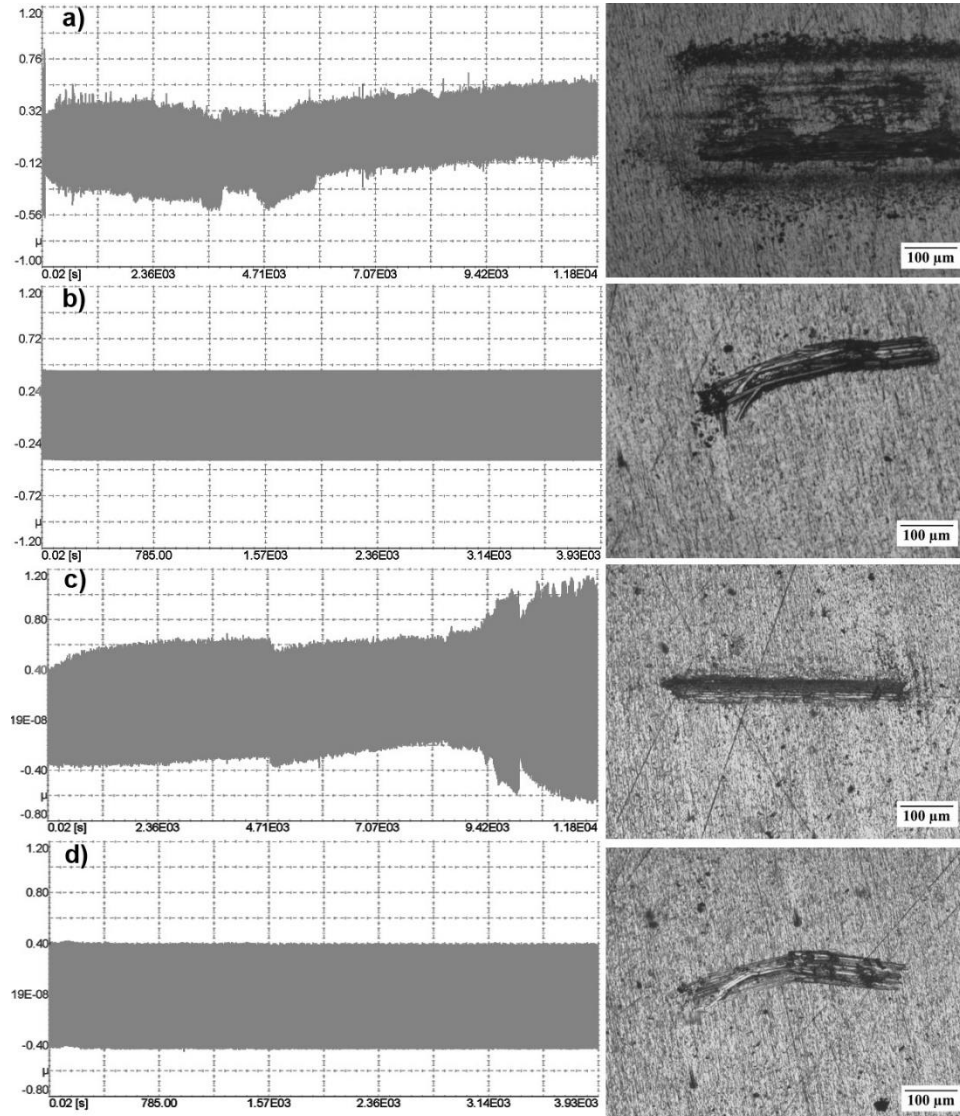speeds (20, 40, 60 N and 0.26, 0.5, 1.0 m/s) resulted in lower friction coefficients (0.40–0.77).

Fig. 4 Sample 3: Dynamic friction coefficient (left) and related wear tracks (right): a) Dry, v=4 mm/s; FN=100mN, b) Dry, v=12 mm/s; b FN=1000mN, c) Ringer, v=4 mm/s; FN=100mN, d) Ringer, v=12 mm/s; FN=1000mN

Our tests also showed a significant decrease of the *COF* values with the load increase (Fig. 7, Sample 2). It can be seen from Fig. 3 that the smallest wear track was exhibited under

the highest load and speed (1000 mN, 12 mm/s) for the wet contact. Severe abrasive wear can be noticed in all the wear tracks.
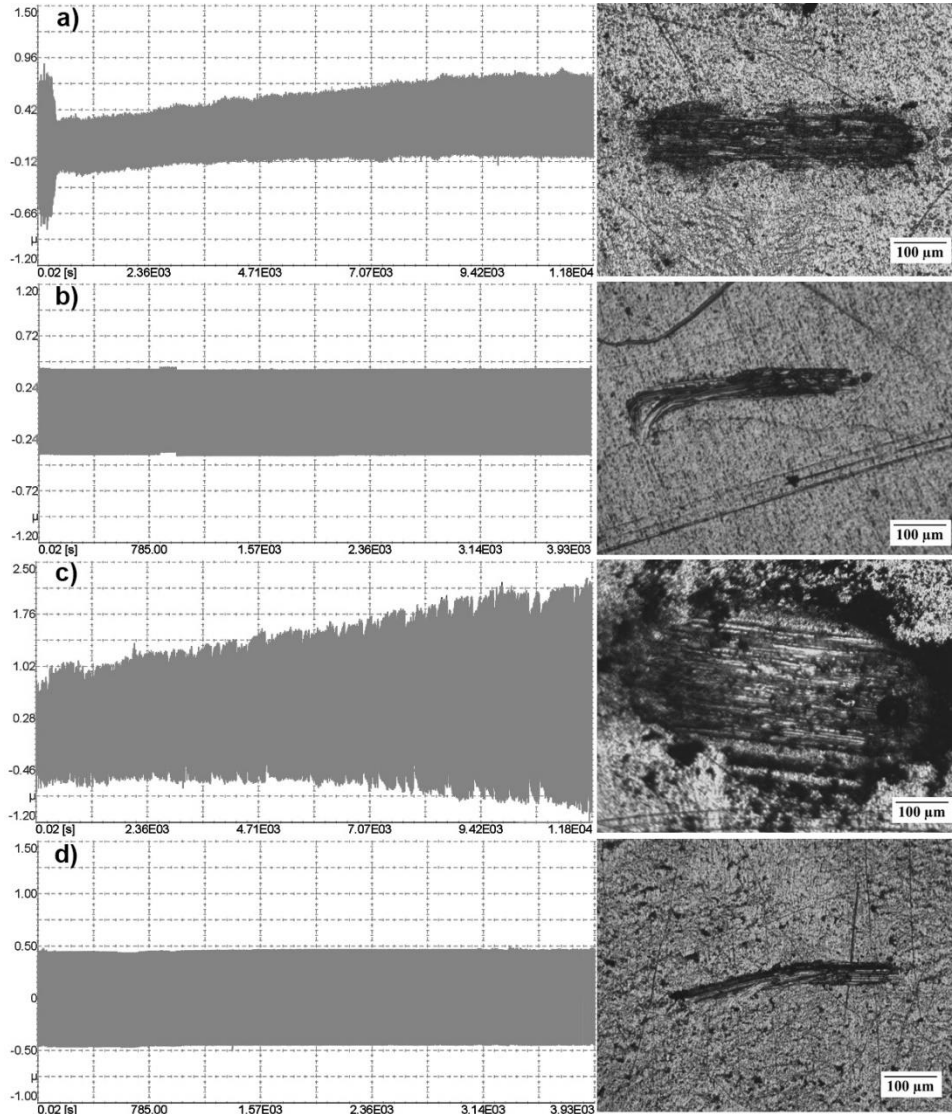

Fig. 5 Sample 4: Dynamic friction coefficient (left) and related wear tracks (right): a) Dry, v=4 mm/s; FN=100mN, b) Dry, v=12 mm/s; b FN=1000mN, c) Ringer, v=4 mm/s; FN=100mN, d) Ringer, v=12 mm/s; FN=1000mN

The lowest *COF* values, as well as wear volumes, and the most uniform behavior, mainly without abrupt variations were produced for Sample 3, what can be seen in Fig. 4. However, severe increase of the *COF* values, almost 2-fold increase, also appeared after

some time, in the case of the presence of the Ringer's solution in the contact zone, under low load and speed (Fig. 4c). It must be noted that the analysis of wear rates presented in [7, 42], showed that with this sample, wet contact produced opposite effect in comparison with the other three types of Ti alloy samples: a lower wear rate was exhibited under the highest load and speed. Simultaneously exhibited high *COF* values with low wear rates indicate probable occurrence of the plastic flow within surface layers of the Ti alloy during the sliding, with severe plastic deformation of layers. From Fig. 4c, it can be seen that the wear track is uniform and small, with deep abrasions only along one inner edge of the track, even though a significant *COF* increase occurred after approximately 20000 cycles.

Sample 4 (Fig. 5) exhibited rather different *COF* behavior than the other three samples. In dry conditions, under low load, the *COF* values were drastically higher during the running-in period, followed by a significant abrupt decrease of the *COF* values that remained low until the end of the test (Fig. 5a). In wet contact, low load produced drastic increase of the *COF* values over time, without any steady state period, and wear track was the largest one of all the tests. Extremely high wear was observed under 100mN and 4 mm/s (Fig. 5c), with calculated wear rate of 2.37×10^{-3} mm^3/Nm [7, 42] and it was significantly larger for wet contacts for all conditions. All Ti samples had wear rates within the range of 10^{-4} - 10^{-5} mm^3/Nm, for almost all regimes of normal loads and sliding speeds, except in these few cases. In general, higher loads produced lower wear rates. Alumina balls also exhibited extensive wear, what is in accordance with research from other authors who studied contacts between alumina and Ti alloys at higher loads than in our study [40, 41].

Values of the efficient friction coefficient, *COF*$_{eff,}$ were calculated for each of the realized tests and their changes are given in Figs. 6 and 7. Variations of the efficient friction coefficient (*COF*$_{eff}$) values, with normal load, for each of the sliding speeds, in dry and wet contacts, are shown in Fig. 6. Changes of the efficient friction coefficient (*COF*$_{eff}$) values, with both normal load and sliding speed, for dry sliding and sliding in the Ringer's solution, for all samples, is shown in Fig. 7, as 3D plots with mapping of the zones is shown in Fig. 8.

From Fig. 6, it can be seen that extremely high *COF*$_{eff}$ values were produced for the lowest load (100 mN) and the highest sliding speed (12 mm/s), in the case of Sample 2. The largest differences of *COF*$_{eff}$ for each sample, were obtained for the lowest load (100 mN), where changes of the sliding speed resulted in a wide range of friction coefficient values, especially pronounced in the cases of Sample 2 and Sample 4.

The lowest values were exhibited in the case of Sample 3, in general. Increase of load resulted in decrease of efficient friction coefficient values for all the samples, and under the highest load (1000 mN), they had very similar values (around 0.3), for all conditions. Samples 1 and 2 both exhibited very high *COF*$_{eff}$ values, especially Sample 2, thus indicating that, in general, annealing of Ti alloy at 1000 °C is not favorable for tribological performance. Also, Sample 4 had high *COF* values, especially for low loads which indicated that quenching in water (rapid cooling) is not favorable from tribological aspects.
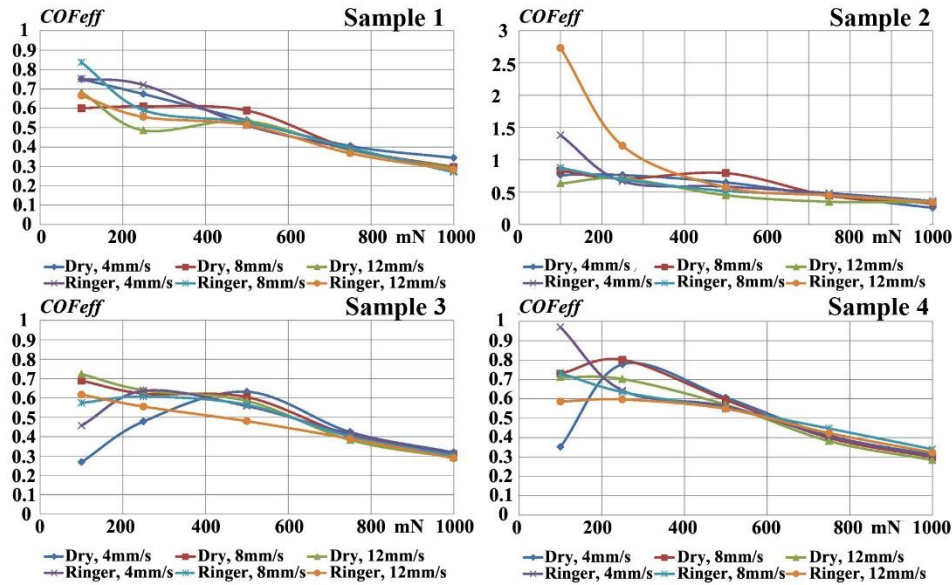
Fig. 6 Variation of the efficient friction coefficient (COF_{eff}), with normal load, for each of the sliding speeds for all samples in dry contact and contact in the Ringer's solution

From Figs. 7 and 8, it can be seen that the sliding speed exhibited complex influence on the COF_{eff} values, for all samples. In the case of Sample 1, the sliding speed had negligible influence on the friction coefficient for all test conditions. A very mild transition can be observed for Sample 1. For the other samples (Samples 2, 3, 4), the sliding speed had pronounced effects under the low loads (100 mN, 250 mN). It can be seen that the change of load resulted in complex responses from aspect of COF_{eff}, similarly to the complex wear behavior as discussed in [7, 42]. The transition nature of the COF_{eff} with the load increase can be seen for all the samples, except in the case of Sample 1, and especially pronounced in the case of Sample 3, for both dry and wet contacts (Figs. 7, 8). In the case of sample 4, the low COF_{eff} values were exhibited for 100 mN, increasing with the load increase up to 500 mN, after which it rapidly decreased with a further load increase to 1000 mN. In the case of Sample 3, the highest COF_{eff} values were exhibited for 500 mN.

This transition behavior is similar to the results of [40], in which dry contact at higher loads (5 - 80 N) and speeds (0.0625 – 1 m/s) is studied. They elaborated that the transition characteristic of load and speed dependence of the dynamic friction coefficient is governed by the elevated temperatures in the contact zone (flash temperatures) and the formation of Ti intermetallics and oxides due to tribochemical reactions. On one side, the increased temperature provokes increase of COF and wear and on the other side, oxides and accumulation of wear debris within the contact zone result in decrease of the contact surface by forming intermediate layers between the Ti alloy and alumina ball. Yang et al., investigated synthesis of TiAl intermetallics on Ti6Al4V by laser modifications and showed that Ti6Al4V reacts with Al to form major hard phases as Ti_3Al, TiAl, and $TiAl_3$, under high temperature [47]. They also showed that wear mechanism associated with TiAl

intermetallics is abrasive wear due to their enhanced micro-hardness. Instability of the friction coefficient and the formation and influence of the third body presence and surface cracks have been also reported for the contact of TiC with alumina ball, where hard debris affected the formation of micro cracks on the surface [48].
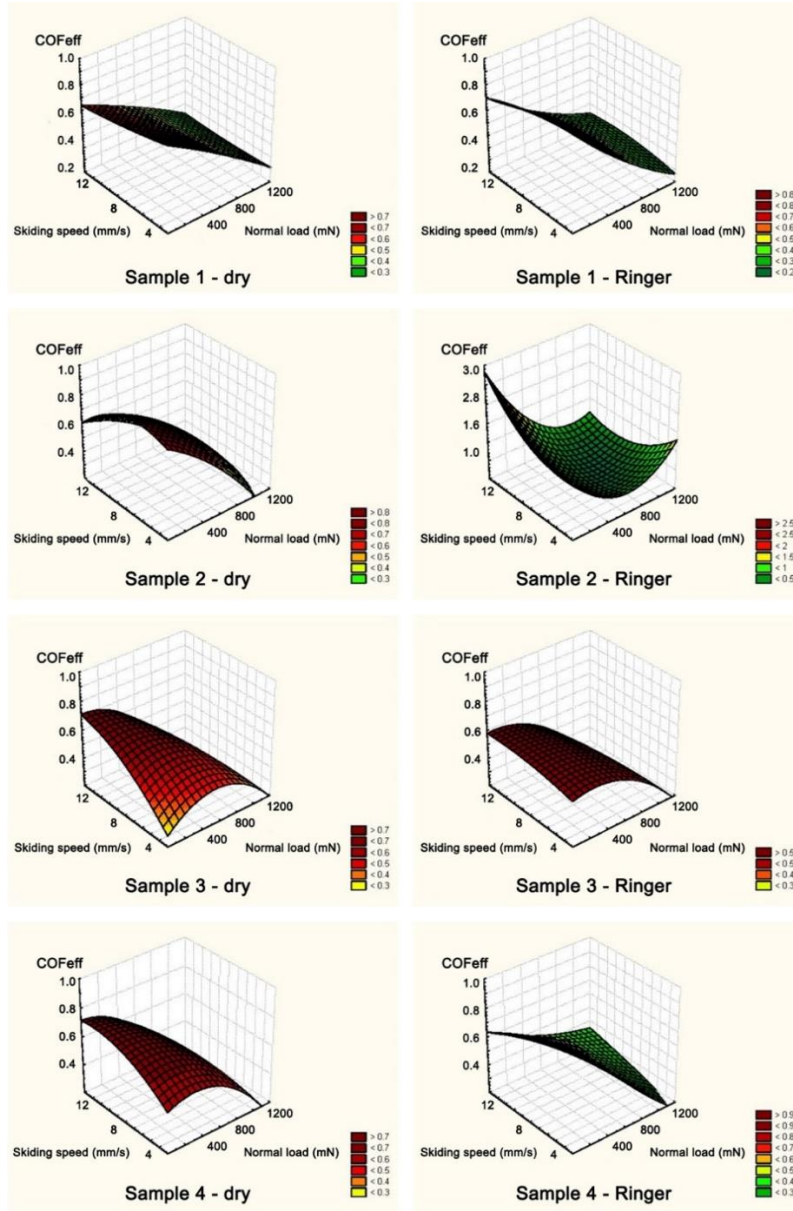

Fig. 7 Variation of the efficient friction coefficient (COF_{eff}), with normal load and sliding speed, for dry sliding (left) and sliding in the Ringer's solution (right), for all the samples

Fig. 8 Mapping of different zones (2D view of the 3D curves shown in Fig. 7): Variation of the efficient friction coefficient (COF_{eff}), with normal load and sliding speed, for dry sliding (left) and sliding in the Ringer's solution (right), for all samples
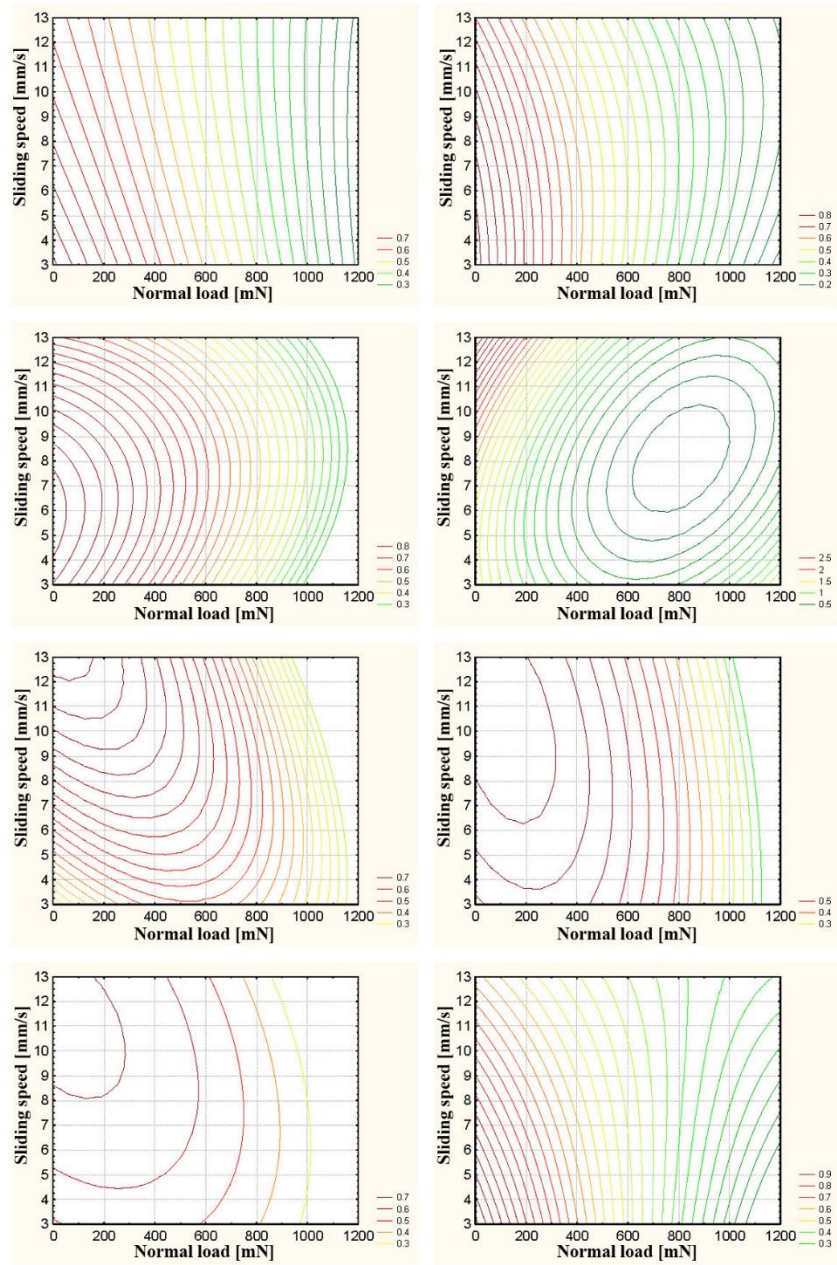
Different microstructures of four samples, as shown in Fig. 9, clearly indicate that their contact behavior was expected to be quite different [23]. The presence of the Ringer's solution additionally changed contact conditions as shown in Fig. 10 and Table 1. In the case of dry contact, the real time unprocessed *COF* diagrams (Figs. 2-5) have many isolated peaks, or sudden changes of the current friction coefficient, thus indicating abrupt changes of the contact conditions at micro scale, considering the nature of the contact pair (Hertzian contact). These sudden changes can result from changes of surface roughness, accumulation (or delamination) of larger quantities of wear debris particles that changes the contact geometry, and appearance of Ti intermetallics and oxides in the contact zone or other chemical processes developing within the contact zone that changes the surface layers of materials in contact. It is obvious that presence of the Ringer's solution rather prevented these sudden changes of the friction coefficient, since all the *COF* diagrams are uniform during the whole test (Figs. 2-5).
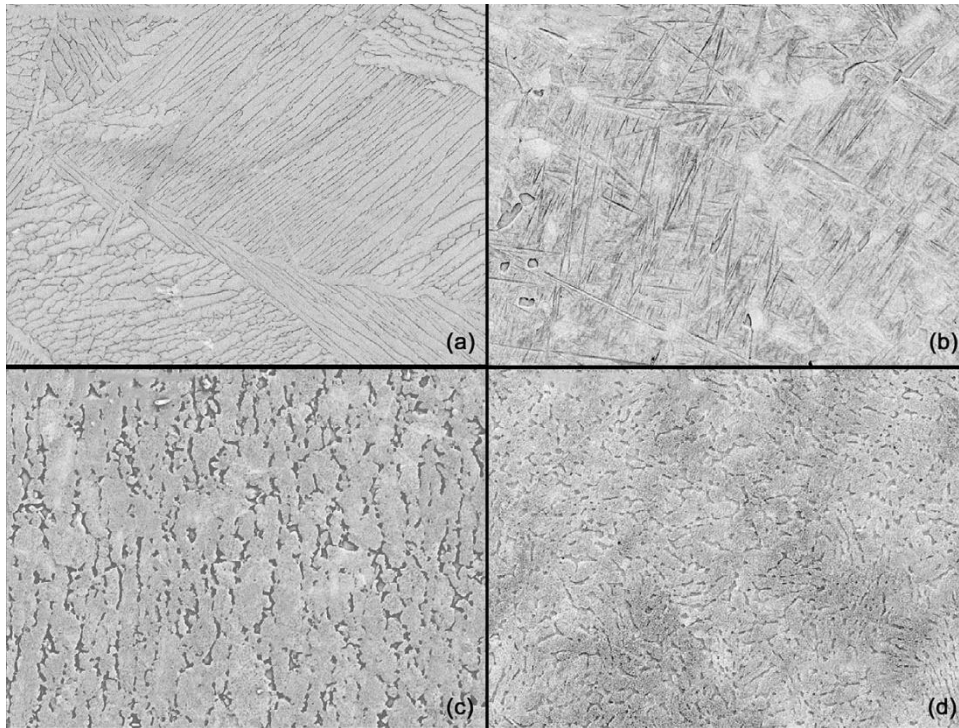

Fig. 9 Microstructures of four samples: a) Sample 1 - annealed at 1000°C; furnace cooled, with fully lamellar microstructure, b) Sample 2 - annealed at 1000°C; water quenched, with martensitic microstructure, c) Sample 3 - annealed at 750°C; furnace cooled, with equiaxed microstructure, d) Sample 4 - annealed at 750°C; water quenched, with globular microstructure

Research showed that lamellar microstructures have better fracture toughness and creep strength, while equiaxed microstructures have better fatigue strength and ductility [12]. Alpha phase is harder than beta phase which is more ductile, but more stable at

temperatures higher than 882°C degrees [13]. We can elaborate that in the case of the microstructures where beta phase is more present (Samples 2, 4), wear behavior of the alloy will be governed by the beta phase wear since it is proven that crack propagation is easier in beta phase [3, 49]. Similarly, alpha phase wear will dominate in the case of the microstructures with a higher amount of alpha phase (Samples 1, 3). However, contact loading together with high flash temperatures during the contact will influence dynamic redistribution of phases during the contact, whereas initial microstructure highly influences the resulting wear mechanisms as well as its extent. Below 882°C degrees, the alpha phase should bear the load as the stronger phase, hence micro-abrasive wear will occur and formation of wear debris. Above 882°C degrees, the beta phase is stable and should bear the load [4, 6], meaning that more micro-deformation of surfaces should occur accompanied with the material flow and lower amount of wear debris.
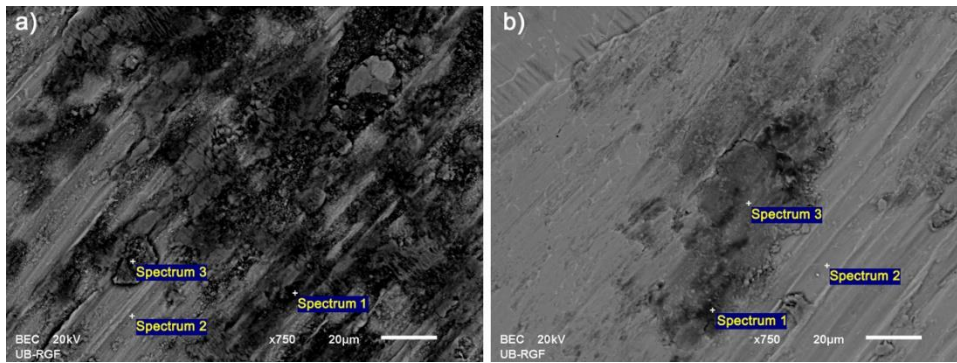

Fig. 10 SEM image of the wear track: a) Dry contact, b) Contact in the Ringers' solution, with positions where EDS analysis was done, as shown in Table 1.

Table 1 EDS analysis realized for zones shown in Fig1, for dry and wet contact: all elements analyzed (in weight %))

Position/ Spectrum	Dry contact				Contact in Ringers' solution						
	O	Al	Ti	V	O	Al	Cl	K	Ca	Ti	V
1	45.68	3.75	48.64	1.93	33.50	1.71	0.54	0.63	0.56	61.3	1.75
2		6.94	90.21	2.85		6.60				90.7	2.67
3	24.73	4.45	67.56	3.26	30.64	2.92	0.20		0.24	64.2	1.79

For the dry contact under low loads and speed (also meaning lower flash temperatures), fully lamellar microstructure (Sample 1) will favor micro-delamination of alpha phase when the direction of contact motion is in line with lamellas, beside the high abrasive wear, what can lead to catastrophic total wear (as shown in Fig. 2a). High load and speed increase flash temperatures, what can cause instability of the alpha phase when beta phase should begin to bear the contact load, thus lowering the total wear, as shown in Fig. 2b. Martensitic microstructure (Sample 2) exhibits irregular alpha/beta distribution what favors high

abrasive wear, preventing micro-deformation or plastic flow, resulting in extensive amounts of wear debris (as shown in Fig. 3a). Equiaxed microstructure (Sample 3) exhibits the highest amount of equiaxed large alpha phase grains where direction of the contact sliding has the lowest influence, with governing abrasive wear at the lowest load and speed and plastic flow at highest load and speed (as shown in Fig. 4a,b). Globular microstructure (Sample 4) exhibits smaller globular alpha phase grains than Sample 3, thus favoring high abrasive and micro-delamination wear, slightly lower under high loads (as shown in Fig. 5a,b). Longer contact time contributes to grain refinement and densification within the surface layers, thus favoring larger wear, what can be seen also in the case of Sample 3 (as shown in Fig. 4a).

From the aspect of wear debris accumulation, the presence of the fluid influences its regular elimination from the contact zone, thus preventing its larger accumulation within the contact zone. However, the Ringer's solution is beneficial for the development of complex chemical interactions between the two materials in contact. That is not a fluid that would promote lubrication and smoother contact, due to the salt crystals ($NaCl$, $CaCl_2$) within its composition that can act like small abrasive particles and third body within a contact zone. It might be elaborated that changes of the *COF* values during the test under dry conditions is mainly influenced by the wear debris behavior within the contact zone and the chemical changes of the surface layers, such as formation of oxides. Formation of oxides during the loaded contact between these Ti alloy samples and alumina has been proven by EDS analysis, shown in Table 1, as well as by other authors [23]. The penetration depth was continuously recorded during the test. Changes of this parameter have a good correspondence with the presence (or absence) of the wear debris within the contact zone, as discussed in [7].

In the case of Sample 2, dry contact, penetration depth steadily rose during the whole test, thus indicating that sudden changes of the *COF* values (Fig. 3a) could be attributed to chemical changes of the surface layers that promoted strong micro-galling between larger portions of surface asperities of Ti alloy and alumina, followed by sudden delamination wear of larger particles (or patches). In the case of Sample 3, dry contact (*COF* diagram in Fig. 4a), penetration depth quickly increased up to around 3500 cycles (to the maximum of 23.8 µm), after which it started to decrease slowly down to 15.6 µm at the end of the test. Altogether, this indicates accumulation of wear debris followed by its periodic elimination away from the contact zone, what is also confirmed by the wear track surrounded by the coarse wear debris (wear track in Fig. 4a). It corresponds to the onset of irregular fluctuations of the *COF* values after approx. 3500 cycles, as shown in Fig. 4a. After approx. 7000 cycles, *COF* values started to slowly increase until the end of the test. In the case of wet sliding (Fig.4b, v=12 mm/s; b FN=1000mN), *COF* values were uniform during the whole test for Sample 3. However, penetration depth in this case showed constant decrease from the beginning (starting value of 0.27 µm), until the end of the test when it reached -1.65 µm. Nanotribometer software denoted penetration depth distance by the negative sign when it shows the distance above the flat surface of the sample. Accordingly, in this case, alumina ball did not penetrate into the Ti sample during the whole test, except very slightly at the very beginning. It might be explained by almost instant formation of the separation layers between the contacting surfaces from the beginning of the test.

Real time *COF* diagrams (Figs. 2-5) can be analyzed in terms of specific periods during one test, especially if compared to the changes of penetration depth during that same test. In the case of dry sliding of Sample 3, three periods can be distinguished: 1) both *COF* and

penetration depth increases (dominant abrasive wear), 2) transition period near the maximum penetration depth values with the onset of *COF* fluctuations (severe delamination starts to dominate, together with tribochemical wear) and 3) *COF* slowly increased and penetration depth slowly decreased, indicating a strong combination of abrasive, adhesive and tribochemical wear with the formation of wear debris and tribochemical layers between the contacting surfaces and periodical ejection of wear debris particles away from the contact zone. For the wet sliding, only uniform *COF* behavior was exhibited, except during the brief running-in period, thus indicating that, in this case, a short period of abrasive wear is followed by the dominant tribochemical wear, due to formation of oxide films on the flat Ti sample surface. Shape of *COF* curves corresponds to the appearance of wear tracks as given in Figs. 11-14, indicating different wear mechanisms during specific periods/phases during one test, what is in consistence with the results of other authors [39, 40], who have also showed periodic changes in wear mechanisms over time. It can be concluded that, in general, different wear mechanisms appeared during one test, with complex influences of coupled abrasive, adhesive and tribochemical wear mechanisms.

Levels of wear rates (discussed in [7, 42]), indicated different wear mechanisms in the case of dry and wet sliding. For *COF* values higher than 1, it is obvious that frictional welding and micro-galling occurred, thus indicating governing adhesive wear. Evidence of abrasive wear is clear in Figs. 2-5 and Figs. 11-14. Formation of new layers between the contacting surfaces that decreased the contact area, was clearly indicated by the decrease of the penetration depth in some periods during the test, as recorder by the nanotribometer. A high friction coefficient under a low sliding speed produced severe wear in the case of both dry and wet sliding, except in the case of Sample 3 for which the wear rates were rather low, especially for wet contact. Tribochemical wear had a significant role under all conditions.

Wear tracks on Sample 1 and Sample 3, for dry and wet sliding under the highest load and speed (12 mm/s and 1000 mN) are shown in Fig. 11. Deep abrasive grooves and large delamination zones are clearly seen. Adhesive wear is more pronounced for Sample 3 where large delamination zones are visible. In the case of Sample 1, abrasive wear with strong influence of third body wear (for dry contact) and tribochemical wear (for wet contact) can be observed. Main difference between dry and wet sliding is the appearance of ragged wave-like forms in the central zone of the wear tracks in the case of dry sliding, which does not exist in the case of the wet sliding for both samples. This difference supports the conclusion that wear debris particles were not present in larger quantities within the contact zone during the wet sliding. For dry sliding, the central zone is probably influenced by the strong third-body wear from wear debris particles within the contact zone. Serrated appearance of the central zone for dry sliding (Fig. 11a, c) is in accordance with periodic abrupt elimination of the wear debris away from the contact zone during a very brief period of time, afterwards replaced with newly formed wear particles. Wear track width for Sample 1 appears smaller than the track width on Sample 3. Wear rates were low for these contact conditions, as shown in [42], being significantly lower for Sample 3 than for Sample 1, thus indicating that plastic flow plays an important part. This is in accordance with influence of high temperature that occurs within the contact zone (flash temperature), especially under high sliding speeds. Increase of temperature has significant influence on the Ti alloy structure favoring plastic flow instead of abrasion and delamination of surface layers. It also promotes mechanical alloying and the formation of the oxide layers which

further promote delamination and surface spalling. Several authors investigated the influence of flash temperatures and TiAl intermetallics on tribological behavior during the contact between Ti alloys and alumina [40, 50, 43].
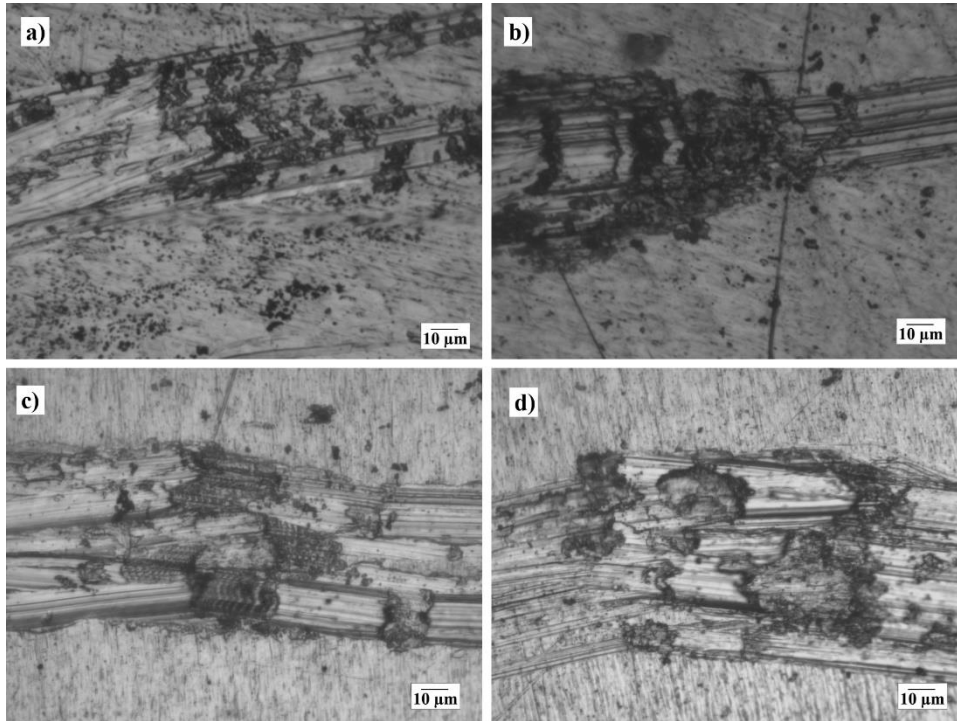

Fig. 11 Wear tracks under 12 mm/s and 1000 mN, on Sample 1: a) dry, b) in the Ringer's solution and Sample 3: c) dry, d) in the Ringer's solution

For similar contact conditions to our tests, contact temperatures within 200 - 350 ℃ range was proved [41]. High temperature significantly influence Ti6Al4V alloy by rapidly decreasing yield strength and resulting in material softening within the limited contact zone [43], what is visible in wear tracks in our tests, too. Plastic deformation was exhibited during the contact between pure Ti and alumina in experimentals performed by [51], who elaborated that the behavior was similar to forming. They also showed that friction coefficient increased over time and associated it with material transfer that occurred during the contact. Studies of the tribo-contact between Ti alloys and steel showed that surface layers of the Ti alloy undergoes significant transformations, with resulting several zones [52]. The authors in this study showed that higher loads resulted in plastic deformation with significant strain levels in localized zones near the Ti alloy surface, which influenced severe wear. Localized plastic strains induce unstable shear and inhomogeneous plastic deformation, thus rapidly decreasing the alloy resistance to deformation and resulting in severe wear onset. Our tests also proved that plastic deformation has an important role in tribological behavior. Additionally, material transfer had significant influence on the contact behaviour, thus influencing complex frictional behavior during the test.

Influence of the sliding speed on tribological behavior was the most prominent under the lowest load (100 mN), where the friction coefficient exhibited widely different values. Wear tracks on Sample 2 in the Ringer's solution and Sample 3 under dry contact for two opposite sliding speeds are shown in Fig. 12. Friction coefficient of Sample 2 in the Ringer's solution was extremely high (around 1.4 in dry sliding and 2.7 in wet sliding) and resulting wear tracks are also large (Fig. 12a, b). Deep abrasive grooves can be seen, with severe pitting throughout the abrasions. Evidence of the plastic flow is visible for wet sliding, while for dry sliding numerous small delamination zones are dominant.
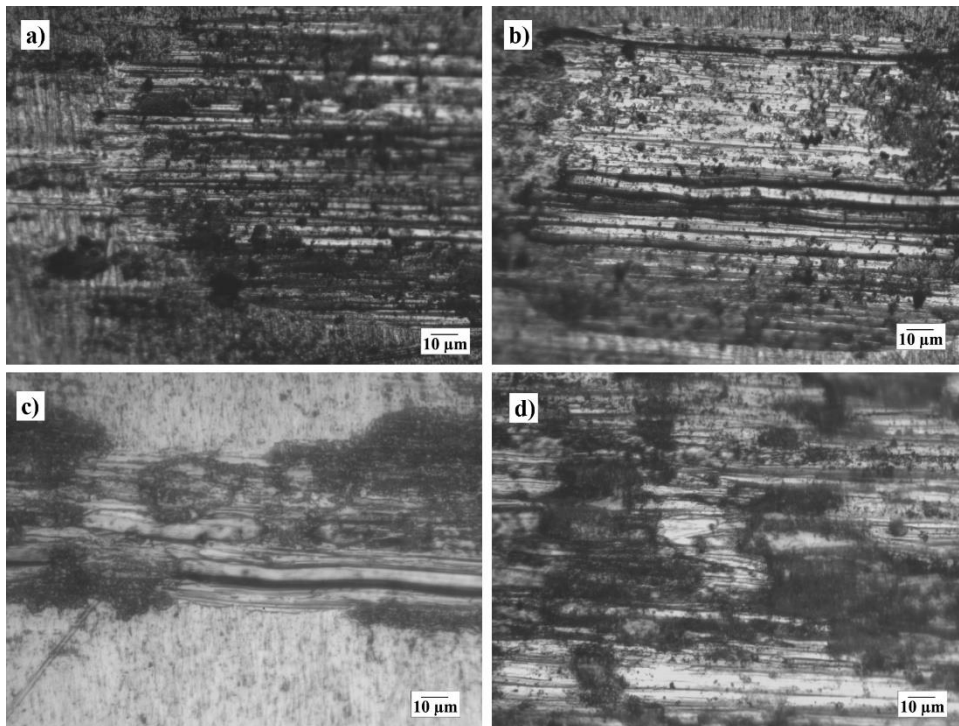

Fig. 12 Wear tracks on Sample 2 at 100 mN load, in the Ringer's solution (a) 4 mm/s, b) 12 mm/s) and Sample 3, dry contact (c) 4 mm/s, d) 12 mm/s)

Appearance of the pitting, especially pronounced in the case of wet sliding is caused by the tribochemical reactions that together with material changes related to mechanical wear, further promote corrosion within surface layers. Both friction coefficients for sample 2, under 4 mm/s, and 12 mm/s, are larger than 1, thus indicating severe galling and frictional welding between the contacting surfaces. Higher wear rate would be expected for 12 mm/s (with *COF* value of 2.7), but it was lower in comparison to the test at 4 mm/s. We can elaborate that such strong adhesive bonding between asperities influenced rearrangement of the surface layers due to plastic flow, rather than its wear, in the case of wet sliding, thus keeping lower wear rates with such high *COF* values. Also, there was probably lack of third-body wear due to the presence of fluid within the contact zone that regularly ejected away wear debris particles. This is also in accordance with existing martensitic

microstructure of sample 2, having hard surface layers that are prone to delamination as shown in [45].

Localized corrosion of Ti6Al4V during the tribocontacts has been studied because it has significant influence on wear mechanisms [18]. Complex corrosion degradation mechanisms were observed on Ti6Al4V surface, as influenced by the material transfer between contacting surfaces, nano and micro frictional welding of asperities during the contact and chemical reactions of Ti alloy with counterbody material, leading to mechanically assisted crevice corrosion, pitting and localized corrosive degradation of surface layers that ultimately can result in fractures. All of these processes are dynamically developing over time during the contact; they are subject of investigations since the mechanisms that influence degradation of hard materials (such as alumina) by softer Ti alloy, are not fully understood. Some researchers showed that significant redistribution of material occurred in subsurface layers of Ti6Al4V during the tribocontacts and produced increase in nano-hardness of transformed layers [53, 54]. Micro-cracking and localized surface strain hardening appeared as the consequence of adhesion and surface plastic deformation preceding wear debris formation [54]. Oxidative processes and chemical reactions between materials in contact additionally influence the wear debris, leading to the formation of fine fully oxidized particles. These microstructural changes within surface layers of Ti6AlV can make them significantly harder than bulk alloy. Sauger et al. [54] showed formation of nano-crystalline structures in surface layers of Ti alloy. Silva et al. [53] showed formation of martensite-rich thin layers in Ti6Al4V under the influence of localized high temperatures. Licausi et al. [55] studied tribocorrosion mechanisms (at 3N load) and showed that wear is in consistence with the Archard law only under initial high contact pressures. For lower contact pressures and presence of the third body they showed that the Archard law is not valid for wear, thus indicating transition and changes of wear mechanisms during the contact, due to tribochemical response. Experimental tribocorrosion study at 8 – 100 N load range that was focused on the influence of the surface roughness, showed that smooth surfaces exhibited more pronounced surface damage and plastic deformation than the rough surfaces due to corrosion attacks [56]. This research also showed that fretting contact initiated crevice corrosion in all the cases of surface roughness, with transition characteristic of the current density during tribocorrosion tests. Transition behavior of wear was also proven for the contact of Ti6Al4V with steel [52].

For sample 3, influence of the speed is obvious if wear tracks in Fig. 12c, d, are compared. Low sliding speed resulted in very low friction coefficient (around 0.27) and high sliding speed exhibited friction coefficient of around 0.72. It was similar also for wet sliding. Wear track at 4 mm/s was small (Fig. 12c) with clear dominant influence of abrasive and tribochemical wear. Adhesive wear can be noticed, but delaminated zones appear as roughened fracture surfaces, probably due to numerous detachments of small wear debris particles and influence of chemical processes that developed during the contact. For higher speed (12 mm/s), delamination zones are significantly larger and almost without roughened fracture surfaces within it (as in the previous case), even though they can be noticed. Direct consequence of the flash temperature within the limited contact zone, beside extensive plastic deformation, is also frictional welding of asperities in contact along with mechanical alloying and galling, what further promotes plowing and delamination. Deep abrasive grooves are broken by delaminated surface layers of larger sizes.

Influence of load was significant on Sample 3, showing transition nature, especially under low sliding speed (Fig. 7). Wear tracks on Sample 3 at the lowest sliding speed

(4mm/s), for different loads, under dry and wet sliding, are shown in Fig. 13. Transition of *COF* values occurred at 500 mN, as shown in Fig. 7. For dry contact, wear track under the lowest load (100 mN) was small, as shown in Fig. 4a and Fig. 12c, and *COF* value was low, as shown in Figs. 6 and 7 (around 0.27). Under 500 mN, adhesive wear started to dominate along with abrasive and tribochemical wear (Fig. 13a). Increase of load to 1000 mN resulted in lower influence of severe adhesive wear which was mainly exhibited in the central zone of the wear track (Fig. 13b).
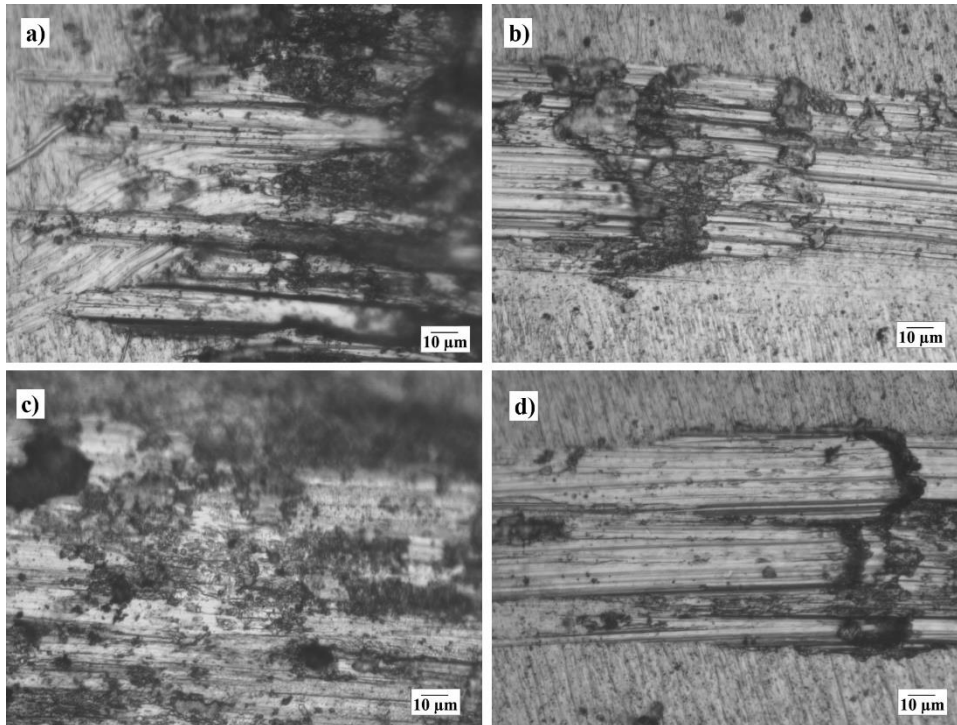

Fig. 13 Influence of load on wear at 4 mm/s sliding speed. Wear tracks on Sample 3: dry contact (a) 500 mN, b) 1000 mN), in the Ringer's solution (a) 500 mN, b) 1000 mN)

For the highest load, abrasive grooves became smooth indicating onset of the plastic flow and smaller amounts of the wear debris in the contact zone. For Sample 3, presence of the Ringer's solution lowered *COF* values, in general. However, at 500 mN, *COF* values were rather high (around 0.6), even though wear rate was low [42]. Corresponding wear track (Fig. 13c) showed shallow abrasive grooves broken by numerous delamination zones appearing as rough fracture surfaces. The highest load (1000 mN) again resulted in low *COF* values and very small wear rates. Corresponding wear track (Fig. 13d) exhibits dominant mild abrasive wear, even though small delaminated zones appeared (mainly in the central zone). In the case of Samples 1 and 2, Cvijovic-Alagic et al. [46] showed that, under high loads (40 N), strain hardening of the surface layers occurred.

This is in accordance with visible delamination of the larger patches in the wear tracks, thus indicating that surface layers had different hardness than those beneath, thus making

them prone to delamination (Figs. 11, 12). Riaz et al. [57] showed that anisotropic surface texture significantly influences levels of wear and corrosion of biomedical Ti6Al4V. Piao et al. [9] investigated thermal softening effect at different strain rates and showed that Ti6Al4V alloy exhibit hardening effect with strain rate increase. Surface texture has significant influence on the resulting friction coefficient, as studied by several authors [58, 59]. They reported significant friction reduction for textured surfaces, up to 50-85% reduction of friction coefficient for differently textured Ti6Al4V contact surfaces. In our tests, there was a significant redistribution of surface layers, thus provoking dynamic changes of Ti6Al4V surface texture within the contact zone which surely had significant influence on friction coefficient, as shown in *COF* diagrams.

Alumina ball was selected as a very hard material that is chemically inert, opposed to Ti alloy that becomes rapidly softer under elevated temperature. Yield strength of Ti6Al4V promptly decreased with temperature increase, as reported in [43]. However, in our tests, alumina ball also endured severe abrasive wear and pitting, as shown in Fig. 14. An exceptionally high friction coefficient was obtained for these contact conditions (Sample 2 in the Ringer's solution, 100 mN, 12 mm/s). Severe transfer of Ti alloy onto the alumina ball developed during this contact. Strong adhesive bonds, galling and frictional welding of contact asperities probably developed under these experimental conditions. Under the lowest load (100 mN), similar wear behavior was exhibited for all contact conditions of Sample 2. Central contact zone of the ball (Fig. 14a) showed severe spalling of its surface layers and deep abrasive grooves can be seen in the vicinity of the central zone (Fig. 14b), also with evidence of mild tribochemical wear. This strongly indicates that very hard TiAl intermetallic were formed during the sliding (as suggested by different authors), and accumulated within the contact zone causing abrasive effects.

Contact geometry of the contact pair allows the largest accumulation of the worn particles within the close vicinity of the central contact point. From Fig. 14b, it can be seen that severe pitting occurred along the rim of alumina ball, thus indicating that it was the line where the most prominent tribochemical reactions appeared between alumina and Ti alloy. This is the thin zone where accumulated wear debris particles were probably arrested during the sliding, even though, at certain moment, they were eliminated from the contact zone, probably when a critical amount had been reached. Our results are in accordance with other authors who experimentally showed that during the contact between Ti alloy and alumina, very sharp and hard TiAl intermetallics formed (Ti3Al), along with Ti oxides (TiO, Ti_2O_3, TiO_2) [40, 41]. Elevated frictional heat supports development of these complex tribochemical reactions. Dominant abrasive behavior was exhibited for the sliding of Ti6Al4V against alumina ball, with strong presence of adhesive and tribochemical wear [39, 40]. For dry sliding, Dong and Bell [40] observed delamination of plates on both Ti6Al4V sample and alumina ball, with appearance of both intergranular and transgranular fracture. They also showed transition nature of load and speed dependence, what is in consistence with our study. Several authors elaborated that wear debris, together with Ti oxides, can form thin layer between the surfaces in contact and lower the wear rate [39, 40, 41]. Contact under the highest load (1000 mN) in our study exhibited the smallest wear tracks, as shown in previous images.
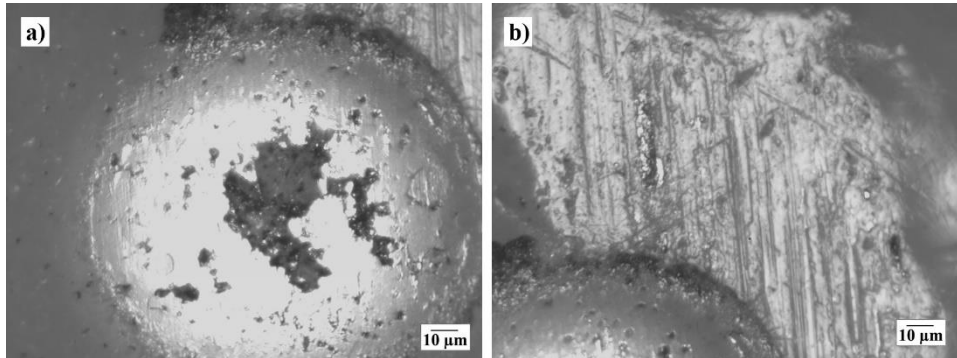
Fig. 14 Wear track on the alumina ball, under 100 mN load and 12 mm/s sliding speed; wet contact with Sample 2: a) central contact zone and b) zone in the vicinity of the central contact zone

In the case of Samples 1 and 2, wear debris around the wear track was coarse, while finer debris particles were generated in the case of Sample 4, with very fine wear debris in the case of Sample 3, thus indicating that heat treatments of Ti alloy samples had very significant effects on tribological behavior. Different heat treatments of Ti6Al4V alloy resulted in completely different microstructure (Fig. 9), as discussed in details in [23]. Our results showed that lamellar and martensitic microstructures were not favorable, neither for wear or frictional response, under low loads and Hertzian contact (ball-on-flat). Namely, both Sample 1 (lamellar microstructure) and Sample 2 (martensitic microstructure) exhibited catastrophic wear and very high friction coefficients in both dry and wet contacts. Lamellar and martensitic microstructure both has lower elastic modulus and yield strength than equiaxed microstructure (Sample 3). This is obviously reflected on friction and wear capabilities of the alloy. On the other hand, a higher presence of Al_2O_3 and V_2O_5 oxides in surface passive layers of Sample 3 and Sample 4 in electrolytic solution is proven [23]. The amount of Al_2O_3 oxides was lower in the case of Sample 3 than Sample 4, leading to the conclusion that these particles also have influence on the friction and wear (Fig. 7), partly due to forming of the passive layer (and increase of corrosion resistance) and in some extent as the third body (and negatively contributes to friction and wear). Tribochemical reactions have important role in tribological behavior of Ti6Al4V – alumina contact and presence of the passive oxide film is of significant influence, as well as the influence of the sharp abrasive TiAl intermetallics. Sample 4 (globular microstructure) exhibited high *COF* values, especially for low loads which indicated that quenching in water (rapid cooling) is not favorable from tribological aspects.

Fan et al. [16] studied the influence of different microstructures of Ti6Al4V on fatigue strength and showed that equiaxed microstructure has the highest fatigue strength, followed by bimodal, lamellar and acicular martensite microstructures, what is in consistence with our results concerning wear. Wear is governed by the damage mechanisms and fatigue strength is of the utmost importance for the endurance of surface layers subjected to external loads. Poor ductility of martensite and lamellar microstructures supports development of cracks under loading, unlike equiaxed and globular microstructures that are beneficial for fatigue resistance. Equiaxed microstructure (as obtained in Sample 3) has the highest ductility, thus promoting plastic flow beside crack initiation and propagation.

Series of thermomechanical treatments on Ti-6Al-4V alloy along with artificial neural network method to correlate microstructure and tensile properties realized by Shi et al. [60], showed that microstructural changes of α and β phases had strong influence on resulting mechanical properties, whereas, β phase had A more prominent effect on tensile properties than α phase. Strong correlation between Ti alloy microstructure and wear resistance, as well as of the energy inputs during the contact, is also showed in experimental study under low load (2 N) [61]. They used first-principles calculations for Gibbs free energy, shear and bulk modulus, in order to evaluate brittle or ductile behavior of different oxides that were formed during the tribo-contact (TiO, TiO_2, Al_2O_3 and V_2O_5 oxides) and showed that these oxides have detrimental influence on the wear resistance of Ti6Al4V alloy in the case of certain microstructural features.

In our tests, Ti6Al4V alloy annealed in Ar at 750 °C and quenched in water, showed the best tribological behavior, with low wear rates, especially in wet contact (of order of 10^{-7} mm³/Nm under high load and sliding speed and with *COF* values mainly around 0.4). Wet contact in our study with the Ringer's solution should represent especially aggressive environment for Ti alloys. However, for Sample 3, presence of the Ringer's solution was beneficial related to friction and wear. Wear of 10^{-4} mm³/Nm belongs to a mild to moderate wear and 10^{-7} mm³/Nm wear rate usually produces wear debris with fine particles and can be associated with tribochemical wear. Microstructural influence is complemented by the appearance of third body in the contact zone. Mechanical alloying and material diffusion between Ti alloy and alumina produce particles that can be incorporated within the soft Ti surface layers, thus promoting dynamic surface modifications during the contact.

Licausi et al. [55] showed that wear cannot be modeled by the Archard law under low contact pressures and with presence of the third body. Dissipative forces, such as friction, depend on the path and are non-conservative forces hence the energy that they take away from the system cannot be restored back. Hence, for conditions of the low loads and very small real contact area, properties of the material surface is of the utmost importance, what, on the other hand, serves as the input to the design process of the anatomical bone structures that are used for modeling, additive manufacturing technologies and reverse engineering [62]. One of the first methods to model wear from the energy point of view was the Reye's method, which proposed that the removed volume of material is proportional to the dissipated energy during the contact [63]. Carpinteri and Pugno [64] proposed wear model based on fractal theory where removed volumes of material has direct dependence on density and hardness of materials in contact. They assumed self-similar distribution of the energy dissipations and developed a model for both brittle and ductile damage mechanisms. Their fractal coupled erosion theory and generalization of the Reye's hypothesis (statistical three-dimensional approach) introduced hardness, density and wear erosion coefficients at micro level, as governing factors for the macroscopic volume of removed materials during the contact. They established clear dependence of the wear resistance as the macroscopic property to the microscopic material constants (hardness, density and wear erosion coefficient). This is fully in consistence with our experimental results where microscopic changes of the material structure in surface layers have essential influence on the wear and friction. We can anticipate that, at any time, at least three different materials, at micro-level, are in contact during the sliding (Ti6Al4V, alumina, Ti oxides, TiAl intermetallics, Ti6Al4V surface nano-crystals, wear debris, the Ringer's solution) with changes over time, due to the complex tribo-chemical reactions. Additionally, Ti6Al4V alloy has pronounced changes of properties with elevated temperature within microscopic zones. Accordingly,

material wear would depend on each of these densities, hardness and wear erosion coefficients, what altogether makes a highly complex system from aspects of wear and friction prediction over time. It could be assumed that microscopic changes of hardness within the localized surface zones on Ti6Al4V, together with its microstructural changes due to the flash temperatures and tribo-chemical processes represent the most influential factors for wear and friction development. Further research should study the possibility to apply the fractal coupled erosion theory proposed by 64.   Carpinteri, and Pugno [64], to the multi-particle system contact at micro-level (consisting of Ti6Al4V, alumina, Ti oxides, TiAl intermetallics, Ti6Al4V surface nano-crystals, wear debris, the Ringer's solution), considering dynamic changes over time, aiming for predictive wear and friction models and a more detailed understanding of the evolving processes during the contact. Artificial intelligence-based models should offer efficient tool for wear and friction prediction over time [65].

4. CONCLUSIONS

Four types of Ti6Al4V alloy exhibited different friction and wear behavior, with more pronounced difference in the case of the dry sliding. Maximum *COF* values in all tests varied within the range of 0.4 – 2.8, indicating that some contact conditions and microstructures produced severe galling and wear. Both friction and wear rate showed transition features, more pronounced for the changes of load than sliding speed, especially in the case of equiaxed microstructure (Sample 3). Dynamic friction coefficient exhibited almost no initial running-in period for all test conditions. The variation of *COF* with material condition and testing conditions were significant. The applied load had more effect on the overall results compared to sliding speed. Sliding speed had lower influence on COF_{eff} for the highest load, for all samples. Sliding in the Ringer's solution, produced fully uniform *COF* curves, unlike significant fluctuations of maximum *COF* values in the case of the dry sliding. Contact conditions at the lowest load (100 mN) and the highest load (1000 mN) exhibited significantly different values for both the friction coefficient and wear. Maximum *COF* values for all Ti alloy samples were significantly larger under low load than at high loads and high speeds. The smallest wear track and the lowest wear volumes were exhibited for the highest load (1000 mN) and sliding speed (12 mm/s), for all samples. Alumina ball also endured severe abrasive wear and pitting. The lowest *COF* values (0.4 – 1.1) were exhibited for the Ti6Al4V sample with equiaxed microstructure (Sample 3), whereas presence of the Ringer's solution was beneficial. However, equiaxed microstructure in Sample 3 also exhibited full transition characteristic for both load and sliding speed, with rather high *COF* values for some contact regimes. Extremely high increase of *COF* values over time, appeared in the case of martensitic Ti alloy microstructure (Sample 2), in dry sliding at low load and speed, with *COF* values reaching 2.8. In general, water quenching was not a favorable treatment for tribological behavior. Lamellar and martensitic microstructures were not beneficial, either for wear or frictional response. Wear mechanisms were governed by the abrasion, delamination, plastic deformation and tribo-chemical reactions.

REFERENCES

1. Geetha, M., Singh, A.K., Asokamani, R., Gogia, A.K., 2009, *Ti based biomaterials, the ultimate choice for orthopaedic implants – A review*, Progress in Materials Science, 54, pp. 397–425.
2. Kanapaakala, G., Subramani, V., 2022, *A review on β-Ti alloys for biomedical applications: The influence of alloy composition and thermomechanical processing on mechanical properties, phase composition, and microstructure*, Proceedings of the Institution of Mechanical Engineers, Part L: Journal of Materials: Design and Applications, 146442072211417.
3. Wang, Y., An, Y., Hou, G., Zhao, X., Zhou, H., Chen, J., 2023, *Effect of cooling rate during annealing on microstructure and ultrasonic cavitation behaviors of Ti6Al4V alloy*, Wear, 204529, pp. 512–513.
4. Gao, P., Fu, M., Zhan, M., Lei, Z., Li, Y., 2020, *Deformation behavior and microstructure evolution of titanium alloys with lamellar microstructure in hot working process: A review*, Journal of Materials Science & Technology, 39, pp. 56–73.
5. Abdalla, A.O., Amrin, A., Muhammad, S., Hanim, M.A.A., 2017, *Effect of heat treatment parameters on the microstructure and microhardness of Ti-6Al-4V alloy*, Proceeding of the 3rd International Conference of Global Network for Innovative Technology 2016 (3RD IGNITE-2016): Advanced Materials for Innovative Technologies, Penang, Malaysia, 030001.
6. Fan, X.G., Meng, M., Gao, P.F., Zhan, M., 2018, *Coupled effects of deformation and cooling on the evolution of primary and secondary alpha of two-phase Ti-alloys*, Materials Science and Engineering: A, 710, pp. 271–279.
7. Zivic, F., Babic, M., S.Mitrovic, Vencl, A., 2011, *Continuous control as alternative route for wear monitoring by measuring penetration depth during linear reciprocating sliding of Ti6Al4V alloy*, Journal of Alloys and Compounds, 509, pp. 5748–5754.
8. Bodunrin, M.O., Chown, L.H., van der Merwe, J.W., Alaneme, K.K., 2019, *Hot working of Ti-6Al-4V with a complex initial microstructure*, International Journal of Material Forming, 12, pp. 857–874.
9. Piao, M., Huh, H., Lee, I., Park, L., 2017, *Characterization of hardening behaviors of 4130 Steel, OFHC Copper, Ti6Al4V alloy considering ultra-high strain rates and high temperatures*, International Journal of Mechanical Sciences, 131–132, pp. 1117–1129.
10. Hémery, S., Naït-Ali, A., Guéguen, M., Wendorf, J., Polonsky, A.T., Echlin, M.P., Stinville, J.C., Pollock, T.M., Villechaise, P., 2019, *A 3D analysis of the onset of slip activity in relation to the degree of micro-texture in Ti–6Al–4V*, Acta Materialia, 181, pp. 36–48.
11. Wendorf, J., Dawson, P.R., Pollock, T.M., 2022, *Grain-Scale Stress States in Microtextured Ti64: Implications for Dwell Fatigue*, JOM: the journal of the Minerals, Metals & Materials Society, 74(19), pp. 3709–3719.
12. Chong, Y., Bhattacharjee, T., Tian, Y., Shibata, A., Tsuji, N., 2021, *Deformation mechanism of bimodal microstructure in Ti-6Al-4V alloy: The effects of intercritical annealing temperature and constituent hardness*, Journal of Materials Science & Technology, 71, pp. 138–151.
13. Chávez Díaz, M.P., Henche, S.A., Yanchuck, M.R., de Arriba, C.C., Sierra, R.C., Rincón, M.L.E., Hallen, J.M., 2022, *Implantation of heat treatment Ti6al4v alloys in femoral bone of Wistar rats*, Journal of Materials Science: Materials in Medicine, 33, 70.
14. Bocchetta, P., Chen, L.-Y., Tardelli, J.D.C., Reis, A.C. dos, Almeraya-Calderón, F., Leo, P., 2021, *Passive Layers and Corrosion Resistance of Biomedical Ti-6Al-4V and β-Ti Alloys*, Coatings, 11, 487.
15. Li, H., Zhao, Z., Ning, Y., Guo, H., Yao, Z., 2018, *Characterization of Microstructural Evolution for a Near-α Titanium Alloy with Different Initial Lamellar Microstructures*, Metals, 8, 1045.
16. Fan, Y., Tian, W., Guo, Y., Sun, Z., Xu, J., 2016, *Relationships among the Microstructure, Mechanical Properties, and Fatigue Behavior in Thin Ti6Al4V*, Advances in Materials Science and Engineering, 2016, 7278267.
17. Zheng, X., Zheng, S., Wang, J., Ma, Y., Wang, H., Zhou, Y., Shao, X., Zhang, B., Lei, J., Yang, R., Ma, X., 2019, *Twinning and sequential kinking in lamellar Ti-6Al-4V alloy*, Acta Materialia, 181, pp. 479–490.
18. Oladokun, A., Hall, R.M., Neville, A., Bryant, M.G., 2019, *The evolution of subsurface micro-structure and tribo-chemical processes in cocrmo-ti6al4v fretting-corrosion contacts: What lies at and below the surface?* Wear, 203095, pp. 440–441.
19. Fouvry, S., Arnaud, P., Mignot, A., Neubauer, P., 2017, *Contact size, frequency and cyclic normal force*

effects on Ti–6Al–4V fretting wear processes: An approach combining friction power and contact oxygenation, Tribology International, 113, pp. 460–473.

20. Takeda, J., Niinomi, M., Akahori, T., Suzuki, Y., Toda, H., 2005, *Microstructure and fretting fatigue characteristics of highly workable titanium alloy with equiaxed α and Widmanstaetten α structure*. Journal of Japan Instituteof Light Metals, 55, pp. 654–660.

21. Fukui, H., Yang, W., Tsuruta, S., Kaikawa, K., Sugimura, A., Takeda, S., Niinomi, M., 2005, *Ambiguous Transition from Fretting to Sliding of Biomedical Alloys*, In: Materials Science Forum, Trans Tech Publications Ltd., Stafa, pp. 2343–2348.

22. Fan, M., Jin, Y., Han, Y., Ma, L., Li, W., Lu, Y., Zhou, F., Liu, W., 2021, *The effect of chemical structure on the tribological performance of perfluorosulfonate ILs as lubricants for Ti-6Al-4V tribopairs*, Journal of Molecular Liquids, 321, 114286.

23. Cvijović-Alagić, I., Cvijović, Z., Bajat, J., Rakin, M., 2016, *Electrochemical behaviour of Ti-6Al-4V alloy with different microstructures in a simulated bio-environment: Electrochemical behaviour of Ti-6Al-4V alloy*, Materials and Corrosion, 67, pp. 1075–1087.

24. Kim, J., Plancher, E., Tasan, C.C., 2020, *Hydrogenation-induced lattice expansion and its effects on hydrogen diffusion and damage in Ti–6Al–4V*, Acta Materialia, 188, pp. 686–696.

25. Ismail, R., Bayuseno, A.P., Fitriyana, D.F., Taqriban, R.B., Muhamadin, R.C., Al Hakim, R.A.N., Siregar, J.P., 2022, *Mechanical properties characterization of Ti6Al4V for artificial hip joint materials prepared by investment casting*, IOP Conference Series: Earth and Environmental Science, 969, 012001.

26. Schuh, A., Bigoney, J., Hönle, W., Zeiler, G., Holzwarth, U., Forst, R., 2007, *Second generation (low modulus) titanium alloys in total hip arthroplasty*, Materialwissenschaft und Werkstofftechnik, 38, pp. 1003–1007.

27. Cortis, G., Mileti, I., Nalli, F., Palermo, E., Cortese, L., 2022, *Additive manufacturing structural redesign of hip prostheses for stress-shielding reduction and improved functionality and safety*, Mechanics of Materials, 165, 104173.

28. Hu, C.Y., Yoon, T.-R., 2018, *Recent updates for biomaterials used in total hip arthroplasty*, Biomaterials Research, 22, 33.

29. Arabnejad, S., Johnston, B., Tanzer, M., Pasini, D., 2017, *Fully porous 3D printed titanium femoral stem to reduce stress-shielding following total hip arthroplasty: Fully Porous 3D Printed Titanium Femoral Stem*, Journal of Orthopaedic Research, 35, pp. 1774–1783.

30. Philip, J.T., Mathew, J., Kuriachen, B., 2019, *Tribology of Ti6Al4V: A review*, Friction, 7, pp. 497–536.

31. Kaoushik, V.M., Nichul, U., Chavan, V., Hiwarkar, V., 2023, *Development of microstructure and high hardness of Ti6Al4V alloy fabricated using laser beam powder bed fusion: A novel sub-transus heat treatment approach*, Journal of Alloys and Compounds, 937, 168387.

32. Jiang, Q., Li, S., Guo, S., Fu, M., Zhang, B., 2023, *Comparative study on process-structure-property relationships of TiC/Ti6Al4V and Ti6Al4V by selective laser melting*, International Journal of Mechanical Sciences, 241, 107963.

33. Malakizadi, A., Mallipeddi, D., Dadbakhsh, S., M'Saoubi, R., Krajnik, P., 2022, *Post-processing of additively manufactured metallic alloys – A review*, International Journal of Machine Tools and Manufacture, 179, 103908.

34. Chassaing, G., Pougis, A., Philippon, S., Lipinski, P., Faure, L., Meriaux, J., Demmou, K., Lefebvre, A., 2015, *Experimental and numerical study of frictional heating during rapid interactions of a Ti6Al4V tribopair*, Wear, 342–343, pp. 322–333.

35. Maio, L., Liberini, M., Campanella, D., Astarita, A., Esposito, S., Boccardi, S., Meola, C., 2017, *Infrared thermography for monitoring heat generation in a linear friction welding process of Ti6Al4V alloy*, Infrared Physics & Technology, 81, pp. 325–338.

36. Schewe, M., Wilbuer, H., Menzel, A., 2021, *Simulation of wear and effective friction properties of microstructured surfaces*, Wear, 203491, pp. 464–465.

37. Coulibaly, M., Chassaing, G., 2018, *Thermomechanical modelling of dry friction at high velocity applied to a Ti6Al4V-Ti6Al4V tribopair*, Tribology International, 119, pp. 795–808.

38. Jedrasiak, P., Shercliff, H.R., McAndrew, A.R., Colegrove, P.A., 2018, *Thermal modelling of linear friction welding*, Materials and Design, 156, pp. 362–369.

39. Masmoudi, M., Assoul, M., Wery, M., Abdelhedi, R., El Halouani, F., Monteil, G., 2006, *Friction and wear behaviour of cp Ti and Ti6Al4V following nitric acid passivation*, Applied Surface Science, 253, pp. 2237–2243.

40. Dong, H., Bell, T., 1999, *Tribological behaviour of alumina sliding against Ti6Al4V in unlubricated contact*, Wear, 225–229, pp. 874–884.

41. Long, M., Rack, H.J., 2001, *Friction and surface behavior of selected titanium alloys during reciprocating-sliding motion*, Wear, 249, pp. 157–167.

42. Zivic F, Babic M, Cvijovic-Alagic I, Mitrovic S, Vencl A, 2011, *Wear Behaviour of Ti6Al4V Alloy Against Al2O3 Under Linear Reciprocating Sliding*, Journal of the Balkan Tribological Association, 17(1), pp. 27-36.

43. Hager, C.H., Sanders, J.H., Sharma, S., 2006, *Effect of high temperature on the characterization of fretting wear regimes at Ti6Al4V interfaces*, Wear, 260, pp. 493–508.

44. Zivic F, Babic M, Mitrovic S, Todorovic P., 2011, *Interpretation of the Friction Coefficient During Reciprocating Sliding of Ti6Al4V alloy against Al2O3*, Tribology in Industry, 33(1), pp. 36-42.

45. Cvijović-Alagić, I., Cvijović, Z., Rakin, M., 2019, *Damage behavior of orthopedic titanium alloys with martensitic microstructure during sliding wear in physiological solution*, International Journal of Damage Mechanics, 28, pp. 1228–1247.

46. Cvijović-Alagić, I., Cvijović, Z., Mitrović, S., Panić, V., Rakin, M., 2011, *Wear and corrosion behaviour of Ti–13Nb–13Zr and Ti–6Al–4V alloys in simulated physiological solution*, Corrosion Science, 53, pp. 796–808.

47. Liu, Y., Liu, W., Ma, Y., Liang, C., Liu, C., Zhang, C., Cai, Q., 2018, *Microstructure and wear resistance of compositionally graded Ti Al intermetallic coating on Ti6Al4V alloy fabricated by laser powder deposition*, Surface and Coatings Technology, 353, pp. 32–40.

48. Harouz, R., Lakehal, A., Khelil, K., Dedry, O., Hashemi, N., Boudebane, S., 2022, *Dry Sliding Friction And Wear of the WC/TiC-Co in Contact with Al2O3 for Two Sliding Speeds*, Facta Universitatis-Series Mechanical Engineering, 20(1), pp. 37-52.

49. Huet, A., Naït-Ali, A., Giroud, T., Villechaise, P., Hémery, S., 2022, *Onset of plastic deformation and strain localization in relation to β phase in metastable β and dual phase Ti alloys*, Acta Materialia, 240, 118348.

50. Li, C.X., Xia, J., Dong, H., 2006, *Sliding wear of TiAl intermetallics against steel and ceramics of Al2O3, Si3N4 and WC/Co*, Wear, 261, pp. 693–701.

51. Heinrichs, J., Olsson, M., Jenei, I.Z., Jacobson, S., 2014, *Transfer of titanium in sliding contacts—New discoveries and insights revealed by in situ studies in the SEM*, Wear, 315, pp. 87–94.

52. Farokhzadeh, K., Edrisy, A., 2016, *Transition between mild and severe wear in titanium alloys*, Tribology International, 94, pp. 98–111.

53. Silva, D., Churiaque, C., Bastos, I., Sánchez-Amaya, J., 2016, *Tribocorrosion Study of Ordinary and Laser-Melted Ti6Al4V Alloy*, Metals, 6, 253.

54. Sauger, E., Fouvry, S., Ponsonnet, L., Kapsa, P., Martin, J.M., Vincent, L., 2000, *Tribologically transformed structure in fretting*, Wear, 245, pp. 39–52.

55. Licausi, M.P., Muñoz, A.I., Borrás, V.A., Espallargas, N., 2015, *Tribocorrosion Mechanisms of Ti6Al4V in Artificial Saliva by Zero-Resistance Ammetry (ZRA) Technique*, Journal of Bio- and Tribo-Corrosion, 1, 8.

56. Hammood, A.S., Thair, L., Altawaly, H.D., Parvin, N., 2019, *Tribocorrosion Behaviour of Ti–6Al–4V Alloy in Biomedical Implants: Effects of Applied Load and Surface Roughness on Material Degradation*, Journal of Bio- and Tribo-Corrosion, 5, 85.

57. Riaz, M.Q., Caputo, M., Ferraro, M.M., Ryu, J.J., 2018, *Influence of Process-Induced Anisotropy and Synovial Environment on Wear of EBM Built Ti6Al4V Joint Implants*, Journal of Materials Engineering and Performance, 27, pp. 3460–3471.

58. Babu, P.V., Ismail, S., Ben, B.S., 2021, *Experimental and numerical studies of positive texture effect on friction reduction of sliding contact under mixed lubrication*, Proceedings of the Institution of Mechanical Engineers, Part J: Journal of Engineering Tribology, 235, pp. 360–375.

59. Hu, T., Hu, L., Ding, Q., 2012, *The effect of laser surface texturing on the tribological behavior of Ti-6Al-4V*, Proceedings of the Institution of Mechanical Engineers, Part J: Journal of Engineering Tribology, 226, pp. 854–863.

60. Shi, X., Zeng, W., Sun, Y., Han, Y., Zhao, Y., Guo, P., 2015, *Microstructure-Tensile Properties Correlation for the Ti-6Al-4V Titanium Alloy*, Journal of Materials Engineering and Performance, 24, pp. 1754–1762.

61. Ju, J., Zhou, Y., Wang, K., Liu, Y., Li, J., Kang, M., Wang, J., 2020, *Tribological investigation of additive manufacturing medical Ti6Al4V alloys against Al2O3 ceramic balls in artificial saliva*, Journal of the Mechanical Behavior of Biomedical Materials, 104, 103602.

62. Turek, P., 2022, *Evaluation of the auto surfacing methods to create a surface body of the mandible model*, Reports in Mechanical Engineering, 3(1), pp. 46–54.

63. Montgomery S, Kennedy D, O'Dowd N., 2009, *Analysis of Wear Models for Advanced Coated Materials*, Matrib: International Conference on Materials, Tribology, Recycling, Croatia, 2009, pp. 1-9.

64. Carpinteri, A., Pugno, N., 2004, *Evolutionary fractal theory of erosion and experimental assessment on MIR space station*, Wear, 257, pp. 408–413.

65. Ribeiro-Carvalho, S., Pereira, R., Horovistiz, A., Davim, J.P., 2021, *Intelligent machining methods for Ti6Al4V: A review*, Proceedings of the Institution of Mechanical Engineers, Part E: Journal of Process Mechanical Engineering, 235, pp. 1188–1210.